AMERICAN ACADEMY OF OPHTHALMOLOGY®

The Topographic Relationships and Geographic Distribution of Prevascular Vitreous Fissures and Cisterns Assessed by Ultrawidefield En Face Vitreous Images

Fei Deng, MD, Mengying Tao, MD, Yanjie Zhu, MD, Xiaoyu Xu, MD, Yue Wu, MD, Lisha Li, Ying Lin, MD, PhD, Yan Luo, MD, PhD

Purpose: To determine the topographic relationships and geographic distribution of prevascular vitreous fissures (PVFs) and cisterns across the entire posterior vitreous membrane in healthy subjects, using ultrawidefield en face and cross-sectional swept-source OCT (SS-OCT) images.

Design: Observational cross-sectional study.

Participants: Ninety-six eyes of 96 healthy participants (age range, 20−49 years) without posterior vitreous detachment.

Methods: For each eye, a 29 × 24-mm SS-OCT volume scan was obtained, along with standardized horizontal and vertical scans through the fovea.

Main Outcome Measures: Ultrawidefield en face and cross-sectional images were analyzed to assess the topographic relationships and geographic distribution of PVFs and cisterns in the posterior vitreous.

Results: En face imaging readily distinguished various preretinal liquefaction spaces throughout the posterior vitreous, extending to near the equator. Aside from the posterior precortical vitreous pocket (PPVP) and the area of Martegiani, all preretinal liquefied fissures and cisterns were distributed along superficial retinal vessels, suggesting they originated from prevascular vitreous liquefaction. In 96 eyes of healthy young and middle-aged adults, PVFs were identified in all participants, presenting a continuous course. Cisterns were detected in 79 eyes (82.3%) and were distributed as follows: superotemporal (91.1%), infratemporal (63.3%), supranasal (41.8%), and inferonasal (22.8%), respectively. The superotemporal cistern was most frequently observed ($P < 0.001$), and cisterns were more likely to involve multiple quadrants with age ($P = 0.005$). Additionally, all preretinal liquefaction spaces, including the PPVP, PVFs, and cisterns, were consistently located overlying the vitreoretinal tightly adhered regions.

Conclusions: Ultrawidefield en face vitreous imaging in healthy young and middle-aged adults revealed that (1) PVFs distributed along superficial retinal vessels with continuous course; (2) cisterns may develop from PVFs and are more common in the superotemporal quadrant; (3) cisterns appear early in life and become more widespread with age; (4) preretinal vitreous liquefaction follows a stereotypic pattern, aligning along regions of firm vitreoretinal adhesion.

Financial Disclosure(s): Proprietary or commercial disclosure may be found in the Footnotes and Disclosures at the end of this article. *Ophthalmology Science 2025;5:100660*

The vitreous is a nearly optically transparent gel structure that fills 80% of the intraocular volume. As individuals age, the volume of the vitreous gel phase decreases while the liquid phase increases.[1] Understanding the anatomical features of the vitreous is essential to grasp the processes involved in vitreous aging and diseases affecting the vitreoretinal interface. However, the transparency and fragile nature of the vitreous make it challenging to study its anatomy.

Previous histological studies have shown that the vitreous has a complex anatomy with numerous fluid-filled spaces that connect and overlap. An optically empty space overlying the macular area has been demonstrated as a uniform finding in human eyes, which was originally described as the premacular bursa by Worst[2] in the 1970s and later renamed as the posterior precortical vitreous pocket (PPVP) by Kishi and Shimizu[3] in 1990 to emphasize the posterior wall of the bursa as the cortical vitreous. The formed vitreous is absent over the optic nerve, and this space is called the area of Martegiani, which extends anteriorly and superiorly through the vitreous cavity to form the Cloquet canal. Ontogenetic theories hypothesize that the Cloquet canal represents the remnants of the fetal primary vitreous. The vitreous cisternal system was firstly proposed by Worst[2,4]

https://doi.org/10.1016/j.xops.2024.100660
ISSN 2666-9145/24

using ink injection technique in autopsy eyes. According to Worst's observations, the vitreous center consists of a core surrounded by 3 separate circles of liquefied cisterns: 72 small cisterns behind the ciliary body, 36 medium-sized cisterns at the equator, and approximately 12 petal-shaped cisterns in the posterior pole. Eisner[5,6] did not report any cisterns, but independently confirmed the presence of prevascular vitreous fissures (PVFs) as areas of optical transparency overlying the superficial retinal blood vessels, theorizing that these spaces might result from an absence of vitreous production. By electron microscopy observation, Sebag and Balazs[7,8] did not document bursa, cisterns, or PVFs but further emphasized the fibrillar nature of the vitreous.

With the advancement of OCT, it is possible to non-invasively visualize vitreous structures in unprecedented detail. OCT has confirmed the presence of PPVP and other liquid structures within the vitreous that were previously identified in cadaver eyes.[9–13] However, studies on PVFs and cisterns remain relatively limited. This scarcity may be due to the unpredictable locations of PVFs and cisterns across a broad area, which makes it challenging to capture these elusive liquified structures with conventional OCT. Using 5-line cross-sectional OCT scans, Pang et al[14] proposed that the cisterns described by Worst may represent age-related liquefied lacunae and that PVFs might be the precursors to cisterns, as both are positioned over superficial retinal blood vessels. While these inferences were previously based on cross-sectional sampling, they can now be more effectively examined using Z-scan visualization techniques.[15]

Z-scans obtained with the latest swept-source OCT (SS-OCT) technology enable comprehensive visualization of complex vitreous fluid spaces. However, earlier en face images were generally limited to the macula and optic disc region. Expanding this analysis to map vitreous liquefaction over a larger area could help unveil the seemingly mysterious veil of vitreous liquefaction. Thus, the purpose of this study was to investigate the topographic relationships and geographic distribution of PVFs and cisterns throughout the posterior vitreous using ultrawidefield (UWF) SS-OCT en face imaging.

Methods

Study Participants

This observational cross-sectional study was approved by the Institutional Review Board at Zhongshan Ophthalmic Center, Sun Yat-sen University (IRB approval number: 2023KYPJ337). Written informed consent was obtained from each participant, and the study adhered to the Declaration of Helsinki and complied with the Health Insurance Portability and Accountability Act.

From August 2023 to May 2024, we enrolled a total of 96 eyes from 96 healthy participants aged 20 to 49 years without posterior vitreous detachment at Zhongshan Ophthalmic Center. Each participant underwent slit-lamp biomicroscopy, indirect ophthalmoscopy, noncontact tonometry, and best-corrected visual acuity testing. Exclusion criteria included any history of eye disease, hyperopia exceeding +3.0 diopters, myopia exceeding −6.0 diopters, and systemic conditions known to affect the vitreous, such as diabetes.

Image Acquisition Protocol

Vitreous images were acquired using the VG200 SS-OCT (Intalight Imaging, Ltd), which operates with a 1050 nm swept-source laser and includes an eye-tracking feature. The scan rate of VG200S is 200 000 A-scans per second, with a depth of up to 9 mm. Axial and lateral resolutions were 3.8 μm and 10 μm, respectively.

Ultrawidefield cube scans of 29 × 24 mm, centered on the fovea, were obtained for each eye, capturing 1024 B-scans (each consisting of 828 A-scans) with an imaging depth of 9 mm. Standardized horizontal (29 mm) and vertical (24 mm) vitreoretinal sections centered at the fovea were also acquired. To optimize the visualization of the vitreous, the retina and choroid were positioned posteriorly within the scan window.

Image Analysis

En face structural slabs of the vitreoretinal interface were generated from 29 × 24 mm cube scans, using the automated internal limiting membrane segmentation as the posterior boundary and −100 μm as the anterior boundary. A dynamic assessment of each image was performed by manually adjusting the slab thickness (100−200 μm) and its distance from the retinal surface, providing a 3-dimensional en face assessment of the posterior vitreous. Brightness and contrast of both en face and cross-sectional images were adjusted to enhance visualization of vitreous anatomical features using Intalight 200's built-in functions.

For each eye, the presence and distribution of PVFs and cisterns across the entire posterior vitreous, within approximately 600 μm depth from the retina, were recorded. The horizontal diameter of the PPVP was measured using the integrated software's built-in caliper tool.

Consistent with the previous description,[14,15] PVFs were defined as slender hyporeflective cavities in the vitreous overlying superficial retinal vessels, while cisterns were defined as larger hyporeflective spaces that could be traced posteriorly to an associated retinal vessel. The supramacular bursa was defined as a more central hyporeflective space anterior to PPVP, which was not correlated with any retinal vessel. Discrepancies in grading were resolved by a senior grader (Y.L.).

Statistical Analysis

Statistical calculations were performed using SPSS software version 27.0 (IBM Corp). Quantitative data were reported as mean ± standard deviation (SD), with normality verified through the Shapiro-Wilk test. One-way analysis of variance was used for quantitative comparisons, and Pearson chi-square test was applied to categorical data. Statistical significance was defined as a P value <0.05.

Results

Study Population

A total of 96 eyes from 96 healthy participants aged 20 to 49 years were included. Demographic and clinical characteristics of the participants are summarized in Table 1.

PVFs Distributed along Superficial Retinal Vessels with Continuous Course

The use of UWF Z-scan visualization enabled us to display the continuous course of PVFs along the superficial major retinal vessels, surrounding the PPVP and preoptic area of

Table 1. Demographic and Clinical Characteristics of the Populations

	20–29 yrs	30–39 yrs	40–49 yrs	Total
Total no. of eyes	35	32	29	96
Age, mean ± SD	26.3 ± 2.5	35.1 ± 3.0	43.7 ± 2.4	34.2 ± 7.2
Female sex, no. (%)	18 (51.4)	15 (46.9)	13 (44.8)	46 (47.9)
Refractor error, mean ± SD	−2.52 ± 2.00	−2.00 ± 1.94	−0.23 ± 0.67	−1.64 ± 1.93
PPVP width, mean ± SD	5478.7 ± 800.8	5846.3 ± 876.3	6358.7 ± 993.8	5845.7 ± 941.2
Presence of cisterns, no. (%)	29 (82.9)	26 (81.3)	24 (82.8)	79 (82.3)
No. of cisterns, mean ± SD	3.34 ± 2.01	2.88 ± 2.16	4.83 ± 2.30	3.65 ± 2.27

PPVP = posterior precortical vitreous pocket; SD = standard deviation.

Martegiani (Fig 1.A1–A4). Prevascular vitreous fissures are located overlying the precortical vitreous, always extending into the vitreous body (Fig 2.A2). Regardless of the presence of established cisterns, PVFs were identified in all participants.

Cisterns Are Continuous with PVFs

Cisterns, wider fluid spaces than PVFs, also followed the path of superficial retinal vessels in en face images (Fig 1.B1–B4). Prevascular vitreous fissures were less common in eyes with more established cisterns. Across the posterior vitreous, all cisterns were continuous with PVFs, often expanding further anteriorly. Some cisterns extended into the deeper vitreous gel beyond the underlying blood vessels, which could be readily distinguished through dynamic en face analysis (Fig 2). A thin layer of cortical vitreous fibers was consistently observed at the posterior boundary of both PVFs and cisterns in sectional B-scans (Fig 2.A2). Of the 96 enrolled eyes, 79 (82.3%) showed cisterns, with prevalence consistent across age groups ($P = 0.982$, chi-square test) (Table 1).

The Absolute Number of Cisterns Increased with Age

Participants in their 20s had an average of 3.34 cisterns (range 1–8, SD 2.01), those in their 30s had 2.88 cisterns on average (range 1–10, SD 2.16), and those in their 40s had 4.83 cisterns on average (range 1–8, SD 2.30). Across all participants, there was an average of 3.65 cisterns per eye (range 1–10, SD 2.27) (Table 1). One-way analysis of variance indicated a statistically significant increase in the number of cisterns with age ($F = 5.59$, $P = 0.005$). Similarly, the PPVP size increased with age ($F = 7.25$, $P = 0.001$) (Table 1).

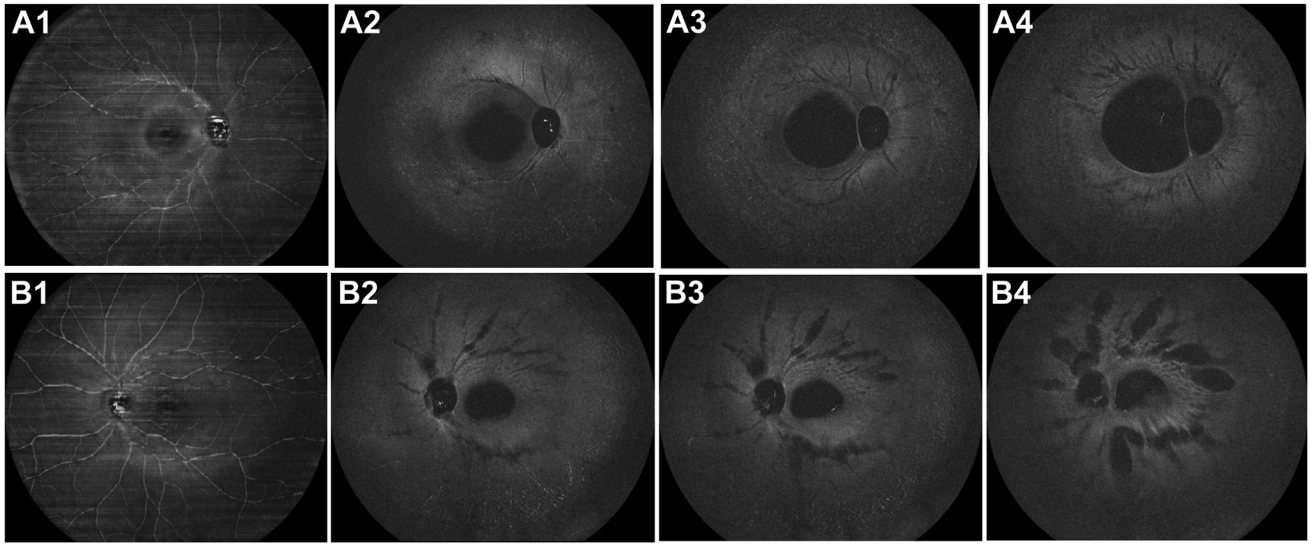

Figure 1. Ultrawidefield dynamic en face assessment of posterior vitreous liquefaction in 2 subjects. (**A1–A4**) 29 × 24 mm dynamic en face scans at (**A1**) 0 μm, (**A2**) 100 μm, (**A3**) 250 μm, and (**A4**) 550 μm anterior to the retinal surface in a 27-year-old myopic (−4.25D) woman show a relatively homogenous vitreous gel structure, with continuous prevascular vitreous fissures (PVFs) overlying retinal blood vessels. Cisterns were not detected. (**B1–B4**) 29 × 24 mm dynamic en face scans at (**B1**) 0 μm, (**B2**) 100 μm, (**B3**) 200 μm, and (**B4**) 450 μm in a 32-year-old myopic (−0.75D) man demonstrate increasing vitreous syneresis with more established cisterns arranged radially and fewer PVFs. Note that cisterns, which are larger than PVFs, are found overlying the same retinal vessel locations. D = diopters.

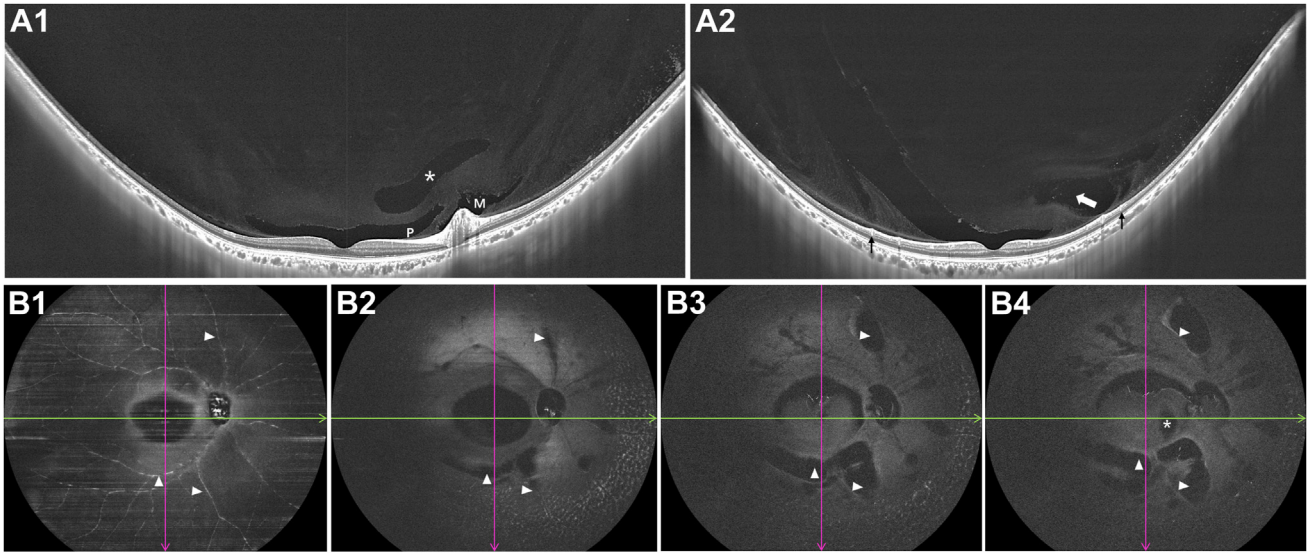

Figure 2. UWF sectional and en face OCT images in a 48-year-old emmetropic man. Horizontal (**A1**) and vertical (**A2**) scans depict a boat-shaped posterior precortical vitreous pocket (PPVP), a conical-shaped area of Martegiani (M), a flat supramacular bursa (white asterisk), with 2 PVFs (black arrow) and a teardrop-shaped cistern (white arrow) overlying 3 retinal blood vessels. A thin layer of cortical vitreous fibers is visible at the posterior border of both PVFs and cisterns. (**B1**–**B4**) 29 × 24 mm dynamic en face scans at (**B1**) 0 μm, (**B2**) 100 μm, (**B3**) 250 μm, and (**B4**) 450 μm anterior to the retinal surface demonstrate the continuous course of PVFs and cisterns of various sizes along the superficial retinal vessels. White triangles indicate noteworthy cisterns expanding anteriorly. The white asterisk in (**B4**) indicates a degenerative supramacular bursa anterior to the PPVP, as shown in (**A1**). Both the PPVP and the area of M are visible in these en face scans. M = Martegiani; PVF = prevascular vitreous fissure; UWF = ultrawidefield.

Cisterns Predominantly Found in the Superotemporal Quadrant

Cisterns were most frequently observed in the superotemporal quadrant, appearing in 72 eyes (91.1%), followed by the infratemporal quadrant in 50 eyes (63.3%), the superonasal quadrant in 33 eyes (41.8%), and the inferonasal quadrant in 18 eyes (22.8%) (Fig 3A). Cisterns in the superotemporal quadrant were significantly more common than in other quadrants ($P < 0.001$, chi-square test), with this distribution pattern remaining consistent across age groups. However, we could only examine the third-order cisterns surrounding the PPVP and preoptic area of Martegiani in the posterior vitreous. As age increased, cisterns appeared in more quadrants, with involvement of all 4 quadrants most noted in participants in their 40s ($P = 0.005$, chi-square test) (Fig 3B).

Consistent Arrangement of Preretinal Liquefaction Structures

Typically, the firm vitreoretinal adhesions are located at the optic disk, the fovea, and along retinal blood vessels. The UWF en face vitreous map revealed that preretinal liquid

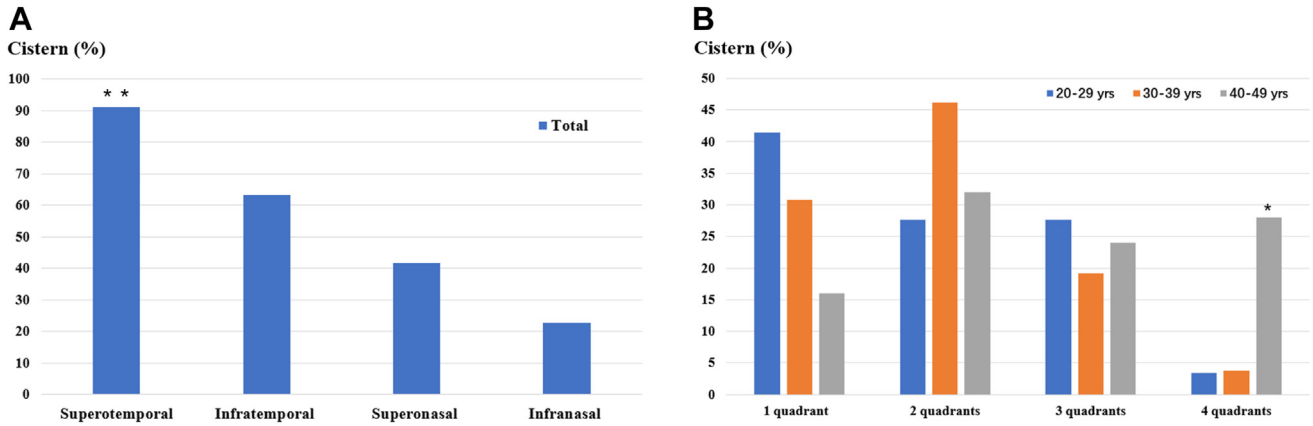

Figure 3. Geographic distribution of cisterns. (**A**) In healthy young and middle aged adults, cisterns were observed most frequently in the superotemporal quadrant (91.1%), followed by the infratemporal (63.3%), superonasal (41.8%), and inferonasal (22.8%) quadrants, with the superotemporal quadrant having the highest incidence ($P < 0.001$). (**B**) Quadrant involvement of cisterns across different age groups shows that cisterns appeared in one or more quadrants, with simultaneous involvement of all 4 quadrants predominantly observed in participants in their 40s ($P = 0.005$). *$P < 0.001$; **$P = 0.005$.

spaces, including the PPVP, PVFs, and cisterns, consistently present overlying these vitreoretinal firm adhered regions. This finding suggests a uniform anatomical arrangement of preretinal liquefaction structures in the posterior vitreous.

Discussion

By using 29 × 24 mm UWF Z-scan visualization method in this study, we were able to display the posterior vitreous liquefaction map in a wide area extending to the vicinity of the equator for the first time, which provides a more comprehensive understanding of vitreous anatomy when put into context with previous studies. As observed by Leong et al[15] and ourselves, PVFs are an almost universal feature of the human eye, probably present at birth. Our findings also support Pang et al's[14] hypothesis that PVFs are the precursors to cisterns, as both structures are distributed along superficial retinal vessels. Additionally, our study confirms Worst's[2,4] findings that various preretinal liquefaction structures are located at predictable sites, though we noted some architectural differences.

Consistent with earlier research,[15] PVFs are found universally in healthy young and middle aged adults, and are always located overlying the precortical vitreous, presenting a continuous course. The alignment of both PVFs and cisterns with superficial retinal vessels further suggests a shared origin in prevascular vitreous liquefaction. With progressive vitreous synchysis and syneresis, PVFs may expand into larger cisternal spaces, as evidenced by fewer PVFs in eyes with more developed cisterns.[14] Notably, our study observed a higher incidence of cisterns (82.3%) compared with previous reports[14] (68%), likely due to the larger area visualized through UWF en face imaging, which allows for a more reliable assessment. Different from Pang et al's observations of cisternal spaces generally not present in young formed vitreous gel, we noted most subjects (82.9%) have manifestations of cisterns at least in their third decade of life. Furthermore, more cisterns were noted with age, and the mean width of the PPVP enlarged as well, supporting the idea that cisterns increase similarly over time.

Ultrawidefield Z-scans gain an advantage to intuitively and comprehensively exhibit the topographic relationship of various vitreous fluid structures to resolve some existing controversies. Earlier studies suggested that some cisterns lack a clear association with specific retinal vessels[14–16]; however, our dynamic en face images consistently revealed that all cisterns are continuous with PVFs, correlating well with the underlying retinal vessels. This discrepancy may stem from the expansion of cisterns to varying widths and depths, with some extending further into the vitreous gel, which might obscure their connection to blood vessels in limited cross-sectional views. Based on the close spatial relationship between PVFs and cisterns, we propose that cisterns develop from PVFs. To emphasize their common origin in prevascular vitreous liquefaction, we suggest renaming cisterns as "prevascular vitreous cisterns."

Cisterns appeared early in life and were found more extensively with age. The distribution of cisterns varied among subjects but was primarily located in the superotemporal quadrant (91.1%), aligning with patterns of early posterior vitreous detachment initiation.[17] Pang et al[14] proposed that the superior location of liquefaction may result from gravitational forces on the vitreous shifting it inferiorly. According to Worst's observations,[2,4] the vitreous cisternal system is hierarchically structured with 72 retrociliary, 36 equatorial, and 12 perimacular cisterns. Due to the limited scan depth of this UWF SS-OCT, we could not assess cisterns near the ciliary body, and equatorial cisterns were also not observed. Consistent with previous findings,[14] most young adults had an average of 3.65 (SD 2.27) posterior vitreous cisterns, with a maximum of 10 identified in this study. The significantly higher count of cisternal spaces observed by Worst might be attributed to the positive pressure of ink injection altering vitreous architecture during dissection.

It has been proposed that vitreous syneresis and synchysis may relate to the vitreous structural organization and the effects of eye movement over decades.[16,17] Eisner[5,6] suggested that PVF development results from a lack of hyalocytes over retinal vessels, which produce vitreous fibrils and secondary vitreous, and experimentally created similar low-density vitreous areas after retinal photocoagulation. However, we noted a thin layer of cortical vitreous fibers at the posterior border, making it doubtful to attribute PVFs solely to absent vitreous production. Gal-Or et al[13] described a dense cortical meshwork of eyewall-parallel fibers over the retinal surface, with perpendicular fibers forming the walls of various vitreous liquid spaces. Considering these observations, we propose that an underproduction of perpendicular fibers over major retinal blood vessels may lead to gaps where PVFs occur, expanding with subsequent syneresis to form cisternal spaces.

Furthermore, the UWF en face map in our study showed that the anatomic arrangement of posterior vitreous fluid spaces (such as PPVP, PVFs, and cisterns) followed a consistent pattern in living eyes, aligning along regions where the vitreous and retina are tightly adhered. While aging contributes to vitreous synchysis and syneresis, it does not entirely explain the stereotypical pattern of liquefaction. Studies indicate that the eye undergoes >100 000 saccadic movements daily, primarily horizontal, over decades, which likely influences vitreous morphology and liquefaction patterns.[18,19] Vitreous collagen fibers adhere to the retina and optic nerve via adhesion molecules such as laminin and fibronectin,[20] with particularly firm adhesion sites located at the optic nerve head, macula, and retinal vessels. Mechanically, saccadic movements transfer angular kinetic energy through these adhesion sites,[21] creating stress that correlates with the locations of vitreous liquefaction. Synthesizing our findings with previous studies, it is plausible that these constant mechanical stresses from ocular saccades may aid to produce this stereotypical liquefaction architectural arrangement, evolving over a lifetime.

This study has several limitations. First, as a cross-sectional study with a relatively small sample size and narrow age range, it is not possible to draw conclusions about cause and effect. A longitudinal prospective study with a wider age range would be beneficial to track the

evolution of PVFs and cisterns over time. Nevertheless, as noted, this was also the main finding of Pang et al,[14] and our results strongly support their interpretation. Additionally, this study represents one of the largest adult cohorts examined regarding vitreous anatomy, spanning 30 years of adulthood. Second, while UWF en face OCT imaging was instrumental in visualizing complex vitreous liquefaction structures, further technological advancements, such as 3-dimensional imaging, would enable quantitative analysis of vitreous fluid spaces.

The Z-scan visualization method is a valuable tool for studying the relationships and distribution of various preretinal vitreous fluid structures. Our study revealed that cisterns are contiguous with PVFs overlying superficial retinal vessels, predominantly in the superotemporal quadrant in healthy young and middle-aged adults. Cisterns appear early in life and become more extensive with age. Additionally, this study demonstrated a consistent arrangement of preretinal liquefaction along regions of strong vitreoretinal adhesion, suggesting that dynamic forces from ocular saccades may contribute to the stereotypic liquefaction patterns. These findings may enhance our understanding of the pathophysiology of vitreous liquefaction and vitreoretinal interface diseases.

Footnotes and Disclosures

Originally received: August 10, 2024.
Final revision: November 18, 2024.
Accepted: November 21, 2024.
Available online: November 28, 2024.Manuscript no. XOPS-D-24-00266.

State Key Laboratory of Ophthalmology, Image Reading Center, Zhongshan Ophthalmic Center, Sun Yat-Sen University, Guangdong Provincial Key Laboratory of Ophthalmology and Visual Science, Guangdong Provincial Clinical Research Center for Ocular Diseases, Guangzhou, China.

Disclosure(s):

All authors have completed and submitted the ICMJE disclosures form.

The author(s) have made the following disclosure(s):

This study is supported by the National Natural Science Foundation of China (Grant No. 81770971), Natural Science Fund of Guangdong Province, China (Grant No. 2024A15150132) to Y.L.

HUMAN SUBJECTS: Human subjects were included in this study. This was an observational cross-sectional study. Institutional Review Board approval was obtained through Zhongshan Ophthalmic Center, Sun Yat-sen University (IRB approval number: 2023KYPJ337). Written informed consent was obtained from each participant. This study complied with Health Insurance Portability and Accountability Act and adhered to the Declaration of Helsinki.

No animal subjects were included in this study.

Author Contributions:

Conception and design: Deng, Xu, Wu, Lin, Luo

Data collection: Tao, Zhu, Xu, Wu, Li

Analysis and interpretation: Deng, Tao, Zhu, Lin, Luo

Obtained funding: Luo

Overall responsibility: Deng, Luo

Abbreviations and Acronyms:
PPVP = posterior precortical vitreous pocket; **PVF** = prevascular vitreous fissure; **SD** = standard deviation; **SS-OCT** = swept-source OCT; **UWF** = ultrawidefield.

Keywords:
Cisterns, En face imaging, Prevascular vitreous fissures, Ultra-widefield, Vitreous.

Correspondence:
Yan Luo, MD, PhD, Department of Ocular Immunology and Uveitis, Zhongshan Ophthalmic Center, Sun Yat-Sen University, 54 Xianlie South Road, Yuexiu District, Guangzhou, 510060 China. E-mail: luoyan2@mail.sysu.edu.cn.

References

1. Tozer KJM, Sebag J. *Vitreous Aging and Posterior Vitreous Detachment. The Vitreous in Health and Disease. 2014*. New York, NY: Springer; 2014:131−150.
2. Worst JG. Cisternal systems of the fully developed vitreous body in the young adult. *Trans Ophthalmol Soc U K (1962)*. 1977;97:550−554.
3. Kishi S, Shimizu K. Posterior precortical vitreous pocket. *Arch Ophthalmol*. 1990;108:979−982.
4. Jongebloed WL, Worst JF. The cisternal anatomy of the vitreous body. *Doc Ophthalmol*. 1987;67:183−196.
5. Eisner G. Biomicroscopy of the peripheral fundus. *Surv Ophthalmol*. 1972;17:1−28.
6. G E. Clinical anatomy of the vitreous. In: Jacobiec F, ed. *Ocular Anatomy, Embryology, and Teratology*. Philadelphia: Harpe & Row Publishers; 1982:391−424.
7. Sebag J, Balazs EA. Human vitreous fibres and vitreoretinal disease. *Trans Ophthalmol Soc U K*. 1985;104:123−128.
8. Sebag J, Balazs EA. Morphology and ultrastructure of human vitreous fibers. *Invest Ophthalmol Vis Sci*. 1989;30:1867−1871.
9. Itakura H, Kishi S, Li D, Akiyama H. Observation of posterior precortical vitreous pocket using swept-source optical coherence tomography. *Invest Ophthalmol Vis Sci*. 2013;54:3102−3107.
10. Schaal KB, Pang CE, Pozzoni MC, Engelbert M. The premacular bursa's shape revealed in vivo by swept-source optical coherence tomography. *Ophthalmology*. 2014;121:1020−1028.
11. Li D, Kishi S, Itakura H, et al. Posterior precortical vitreous pockets and connecting channels in children on swept-source optical coherence tomography. *Invest Ophthalmol Vis Sci*. 2014;55:2412−2416.
12. She X, Ye X, Chen R, et al. Characteristics of posterior precortical vitreous pockets and cloquet's canal in patients with myopia by optical coherence tomography. *Invest Ophthalmol Vis Sci*. 2019;60:4882−4888.
13. Orly Gal-Or QG, Dolz-Marco R. Michael Engelbert in vivo imaging of the fibrillar architecture of the posterior vitreous and its relationship to the premacular bursa, Cloquet's canal, prevascular vitreous fissures, and cisterns. *Graefes Arch Clin Exp Ophthalmol*. 2019;257:709−714.
14. Pang CE, Schaal KB, Engelbert M. Association of prevascular vitreous fissures and cisterns with vitreous degeneration as

assessed by swept source optical coherence tomography. *Retina*. 2015;35:1875−1882.
15. Belinda CS, Leong SF, Kaden TR, et al. OCT en face analysis of the posterior vitreous reveals topographic relationships among premacular bursa, prevascular fissures, and cisterns. *Ophthalmol Retina*. 2020;4:84−89.
16. Spaide RF, Valmaggia P, Maloca PM, et al. Sophie Caujolle Imaging the vitreous with a novel boosted optical coherence tomography technique. Vitreous degeneration and cisterns. *Retina*. 2022;42:1433−1441.
17. Tsukahara M, Mori K, Gehlbach PL, Mori K. Posterior vitreous detachment as observed by wide-angle OCT imaging. *Ophthalmology*. 2018;125:1372−1383.
18. Spaide RF. Visualization of the posterior vitreous with dynamic focusing and windowed averaging swept source optical coherence tomography. *Am J Ophthalmol*. 2014;158:1267−1274.
19. Ibbotson M, Krekelberg B. Visual perception and saccadic eye movements. *Curr Opin Neurobiol*. 2011;21:553−558.
20. Uemura A, Nakamura M, Kachi S, et al. Effect of plasmin on laminin and fibronectin during plasmin-assisted vitrectomy. *Arch Ophthalmol*. 2005;123:209−213.
21. Sebag J. Vitreous and vitreoretinal interface. In: Schachat AP, ed. *Ryan's Retina*. 6th ed. Amsterdam, The Netherlands: Elsevier; 2018:544−581.